



3D Simulation of Enhanced Lateral Drift (ELAD) Sensor

Weijian Lin, Smith College, Northampton, USA

Supervisor: Anastasiia Velyka

September 5, 2018

Abstract

Enhanced lateral drift (ELAD) sensor is a new tracking sensor that can improve position resolution by the lateral drift of charged particles resulting from the non-homogeneous electric field in horizontal direction inside the silicon sensor. This report illustrates the simulation studies of ELAD sensors. The studies are conducted by building the 3D structure of different layers of deep implants in the sensor and getting electric field profile with the Technology Computer-Aided Design (TCAD) SYNOPSIS.

Contents

- 1 Introduction** **3**

- 2 Background** **3**
 - 2.1 Idea of ELAD sensors 3
 - 2.2 TCAD SYNOPSIS 6

- 3 Structure setup and Simulation** **7**
 - 3.1 3D Structure of ELAD sensor 7
 - 3.2 Simulations 12

- 4 Summary and Future steps** **15**

- 5 Acknowledgement** **15**

1 Introduction

In order to obtain information of particles with higher accuracy, particle physics experiments are in need of tracking detectors with higher position resolution. There already exist many methods to improve the position resolution of tracking sensors. One of the most straight forward way is to make sensors with smaller readout cells, but this creates more readout channels within a constant sensor area, which would require higher readout bandwidth from the detector. [1]

In the new concept of enhanced lateral drift (ELAD) sensors, higher position resolution is achieved by an effect called charge sharing. The electric field changes inside the silicon bulk by layers of deep implants, which have different doping concentrations regard to the bulk concentration. The non-homogeneous electric field causes charged particles to change drift path. This report includes the structure schematics of the ELAD sensor and the simulations of the resulting electric fields.

2 Background

2.1 Idea of ELAD sensors

Silicon has become the most commonly used material for high-precision detectors nowadays. A silicon detector works like a reversed biased p-n junction. An external voltage is applied by connecting p-region to the negative terminal and n-region to the positive terminal. As a result, the electrons and holes in the sensor move towards the electrodes and a depletion area with no current flow is formed. The width of the depletion area is given by:

$$w_{depl} = \sqrt{2\varepsilon\mu r V_{depl}} \quad (1)$$

In order for the sensor to function properly, the external voltage needs to be sufficient to deplete the whole volume of the sensor, and the required value is called depletion voltage. [3]

When a traversing particle moves through the depleted volume inside the sensor, it creates free electron-hole pairs (charge carriers). In Figure 1 the kinetic energies of charge carriers are shown in the band representation of silicon structure. [2] The presence of an electric field E will make these electrons and holes drift along the electric field lines. The number of electron-hole pairs created depends on the energy of the traversing particle and the material it is moving through, and in this report we focus on MIPs (Minimum Ionizing Particles) that have the lowest energy loss. [3] The drifting charge carriers are collected by readout electrode strips, and, by the electrode signal, the position of the particle can be reconstructed.

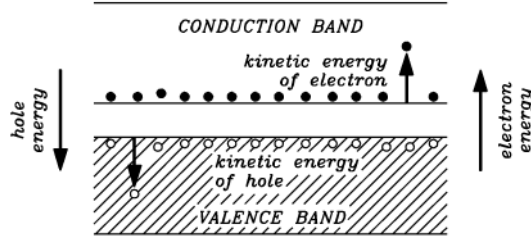


Figure 1: Energy of charge carriers in the band representation

In a standard planar sensor shown in Figure 2, most of the charge carriers are collected on one single readout strip. In this case, the binary resolution of the sensor:

$$\sigma_{bin} = \frac{w}{\sqrt{12}} \quad (2)$$

is only proportional to pitch size w , which is the distance between two adjacent readout electrodes. [4] Therefore the most common way to improve position resolution for this type of sensor is to change the pitch size. Charge carriers moving in the left (right) half area of the pitch will be collected by the left (right) strip. Only the charge carriers moving close to the center of the pitch are collected by both strips.

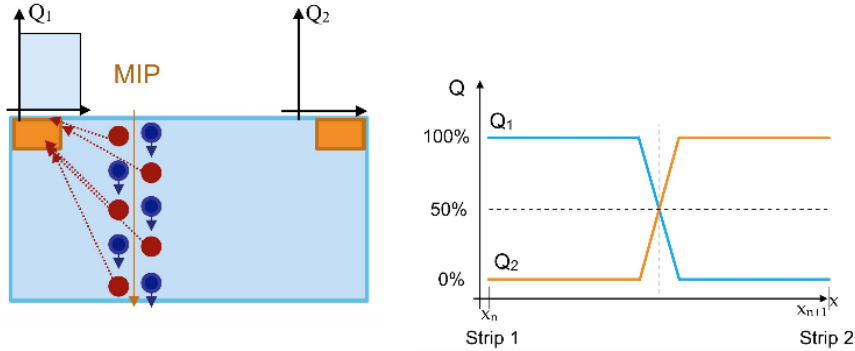


Figure 2: Charge carrier distribution in standard planar sensor

In an ELAD sensor shown in Figure 3, on the other hand, charge carriers are forced to change their drift paths. The electric field inside the sensor is changed by adding deep implants with higher doping concentrations. For example, p^+ -implants in a p-bulk create repulsive (attractive) areas for electrons (holes). [4] The combination of p-implants and n-implants leads to a controllable effective doping concentration, which then leads to a controllable depletion voltage:

$$N_{eff} = N_D - N_A \quad (3)$$

$$V_{depl} = \frac{q_0 D^2 |N_{eff}|}{2\epsilon_r \epsilon_0} \quad (4)$$

where N_A and N_D are acceptor (Boron atoms in p-implants) and donor (Phosphorus atoms in n-implants) concentrations, and D is thickness of the sensor. Both p-implants and n-implants are included in the ELAD sensor in order to keep N_{eff} , and consequently V_{depl} , from getting too high. [1] When the external applied voltage is too high, electric field in the sensor will become strong enough to cause the break down of depletion area and generation of high current. To operate the sensor in a depleted way, breakdown voltage should be far enough from depletion voltage. [3]

Figure 4 shows the 2D simulation of the electric field in horizontal direction inside a standard planar sensor and an ELAD sensor (p-ELAD, structure described in section 3.1). It is clear that ELAD sensor has alternating electric fields. When drifting electrons meet the alternating electric fields created by the deep implants, they change their path laterally. Such effect, accompanied by careful placement of deep implants, can achieve a linear relationship between charge sharing and the position of the traversing particle, which means no matter where the measured particle is, the charge carriers it creates will be collected, with location-specific proportions, by two readout strips. With signals from two readout strips instead of one, the position of the measured particle can be reconstructed more accurately. Figure 5 shows the 2D simulation of the drift path of charge carriers created by MIP inside an ELAD sensor. Charge carriers do change their path and are collected by two adjacent readout strips.

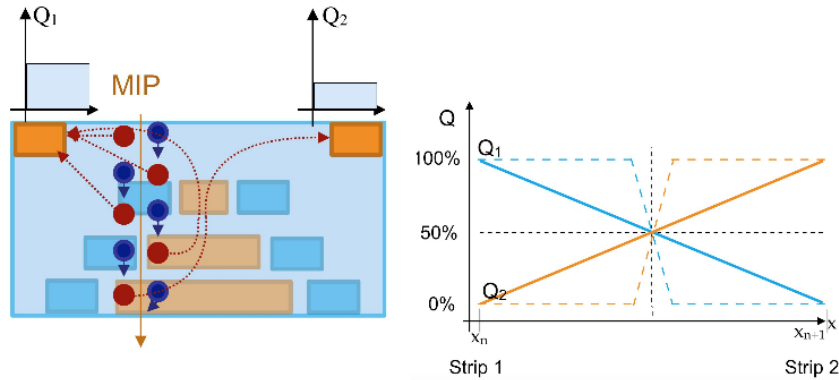


Figure 3: Charge carrier distribution in ELAD sensor (theoretical optimum)

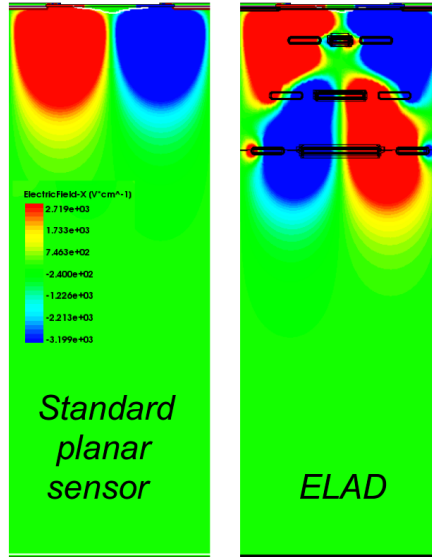


Figure 4: 2D electric field simulation of standard planar sensor and ELAD sensor

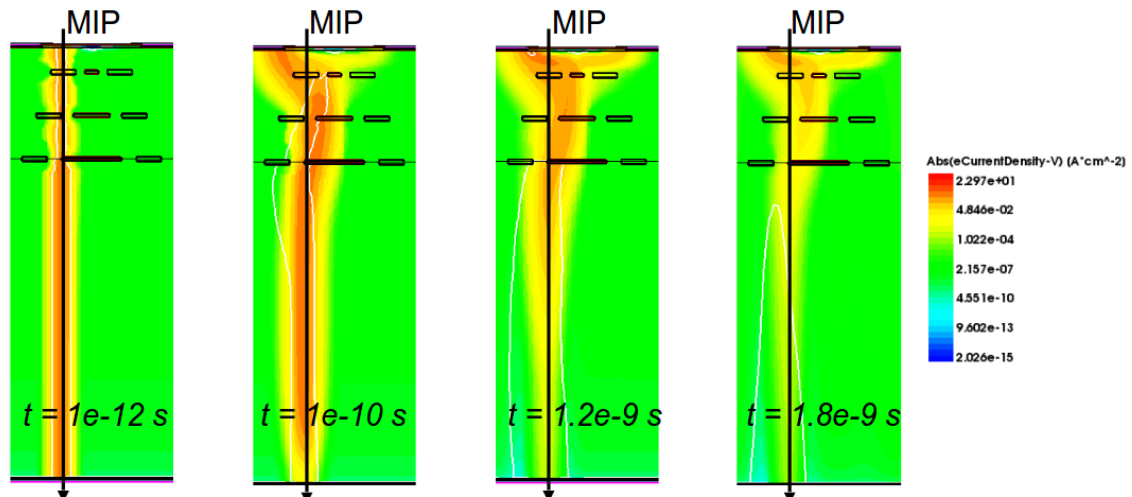


Figure 5: 2D drift simulation with MIP

2.2 TCAD SYNOPSIS

The simulation of the new ELAD sensor is done by the Technology Computer-Aided Design (TCAD) SYNOPSIS, which is widely used for development of semiconductor devices and related technologies. For this project, two tools have been utilized: SDE and SDEVICE. The geometric structures of the ELAD sensor are built by SDE, and the electrical characteristics of the sensor are simulated by SDEVICE. [1]

3 Structure setup and Simulation

3.1 3D Structure of ELAD sensor

For this project two types of ELAD sensors were built using the SDE tool of TCAD SYNOPSIS: n-in-p (p-ELAD) and p-in-n (n-ELAD). Figure 6 shows the 2D cross section of the p-ELAD sensor, which includes the readout electrodes, the readout implants, the SiO₂ layer (on top of p-spray layer), the p-spray isolation, three layers of p- and n-deep implant strips, and backplane. The first and second layer of implants locate in the epitaxial zone due to production technique. The p-spray layer prevents electrons from accumulating below the SiO₂ layer. The total sensor thickness is 150 μm. The pitch size is 55 μm and the readout implant size is 20 μm × 20 μm to accommodate the TimePix3 readout chip, which is planned to be used for the prototype sensors. In a n-ELAD sensor the major structure is the same as the p-ELAD sensor, except the doping profiles are switched, i.e. n- implants in p-ELAD sensor become p- implants in n-ELAD sensor, and there is no p-spray isolation.

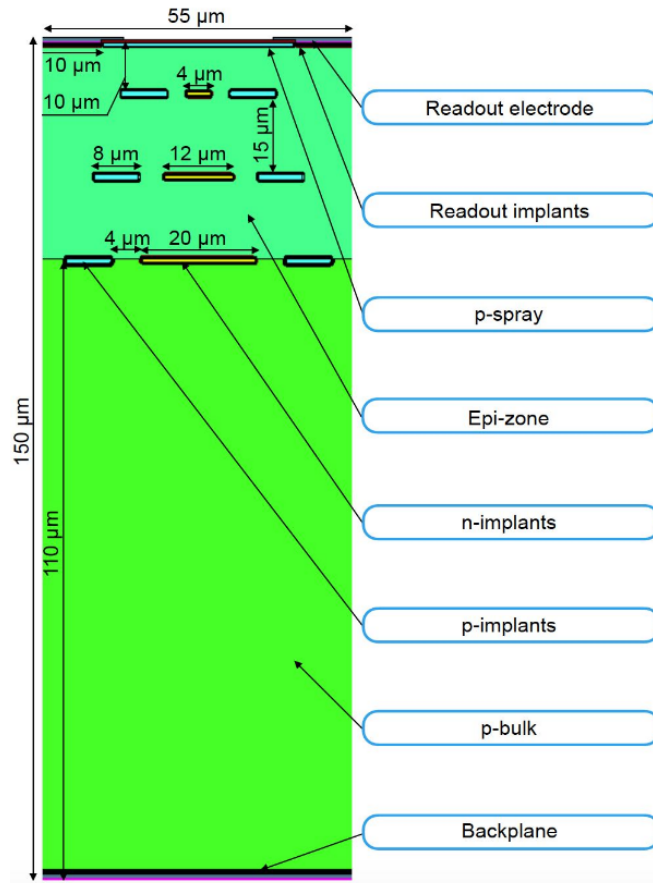


Figure 6: 2D structure of p-ELAD sensor

For both types of the sensor, 2D simulations show that for each implant concentration it is necessary to know the optimal operating voltage. In case of operation voltage 400V, the deep implant concentration should be around $3E+15 \text{ cm}^{-3}$ in order to have the linear contribution between two readout cells (Figure 7). The deep implant concentration cannot be too high either so there is enough difference between depletion and breakdown voltage.

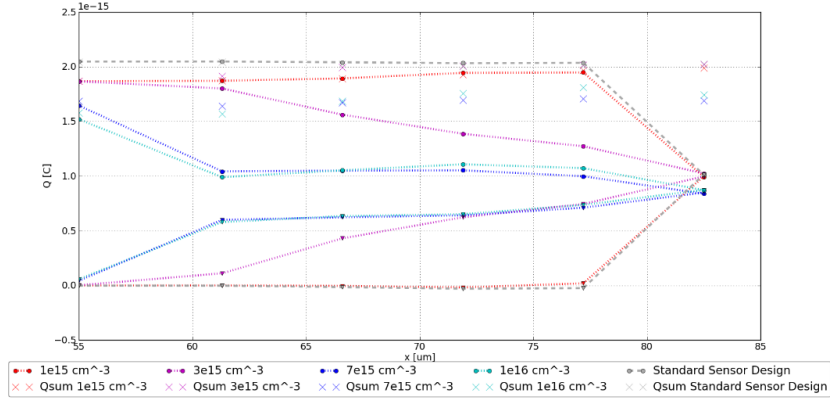
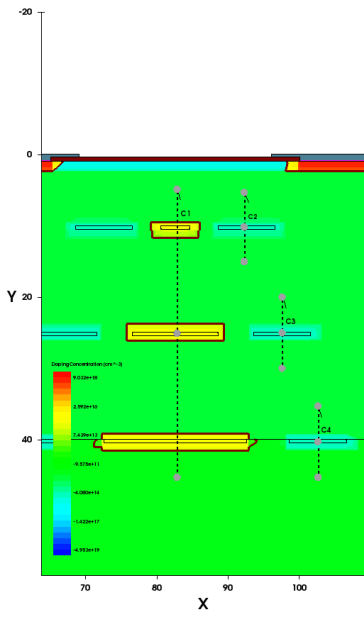
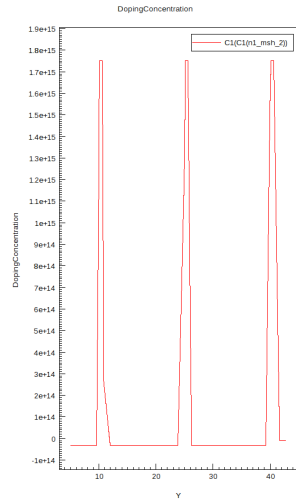


Figure 7: Collected charge on 1st and 2nd strip in the range between half of the strip and half of the pitch

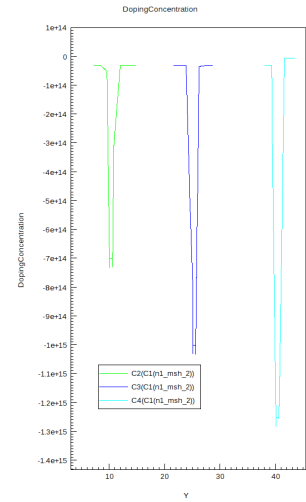
The first 3D ELAD sensor structure is a 5×5 p-ELAD sensor. The doping concentrations of deep implants are shown in Figure 8. All three layers of n-implants share the same concentration, while concentration of p-implants increases with depth to balance concentration between p- and n-implants. Figure 9 and Figure 10 show the structure both in 3D and 2D, as well as the meshing of the implants.



(a) p-ELAD cutline



(b) n-implant concentration



(c) p-implant concentration

Figure 8: deep implant concentrations of p-ELAD sensor

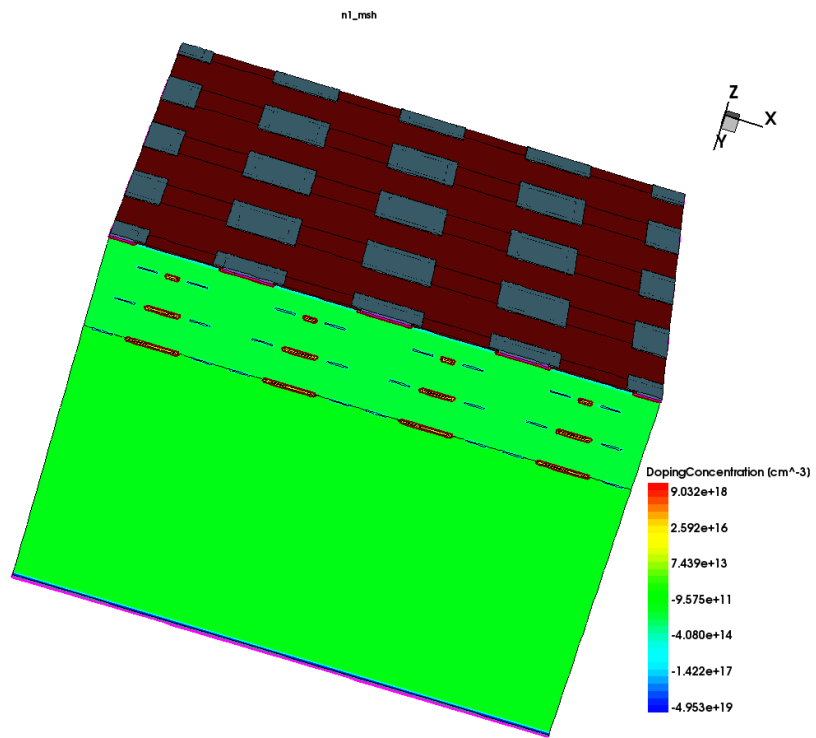


Figure 9: 3D structure of 5x5 p-ELAD sensor

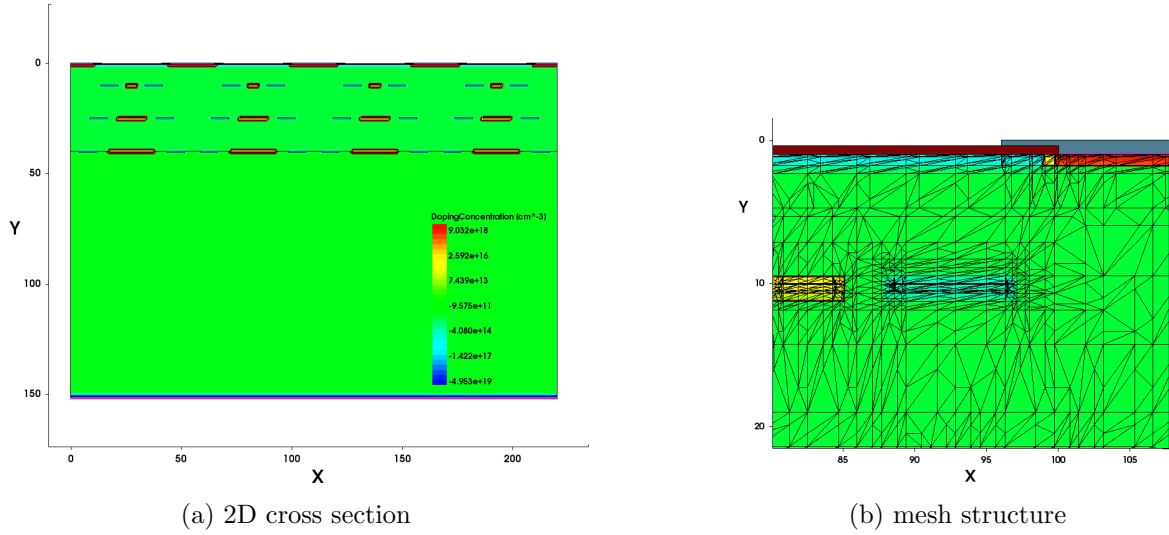


Figure 10: 2D cross structure and mesh of 5×5 p-ELAD sensor

The second 3D ELAD sensor structure is a 5×2 n-ELAD sensor. The doping concentrations of deep implants are shown in Figure 11. All three layers of p-implants share the same concentration (small difference between first two layers and the third caused by difference between epi-zone and n-bulk concentrations), while concentration of n-implants increases with depth. Figure 12 and Figure 13 show the structure both in 3D and 2D, as well as the meshing of the implants. Since further simulations are conducted with this structure, the total volume (number of readout implants) is smaller than the p-ELAD sensor in order to shorten the simulation process time, and the meshing is finer for higher accuracy.

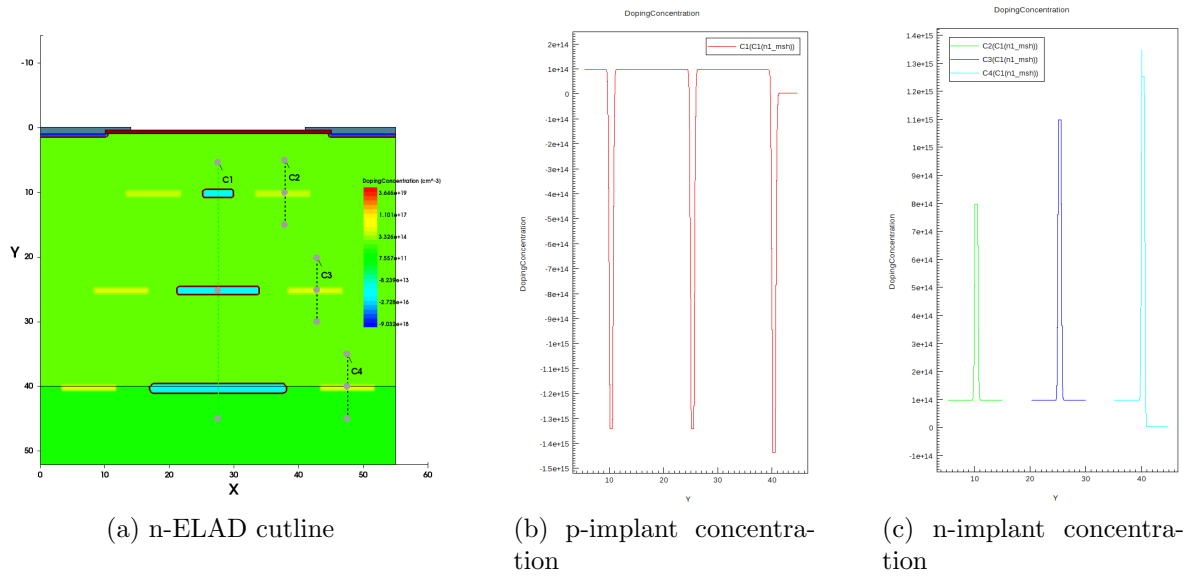


Figure 11: deep implant concentrations of n-ELAD sensor

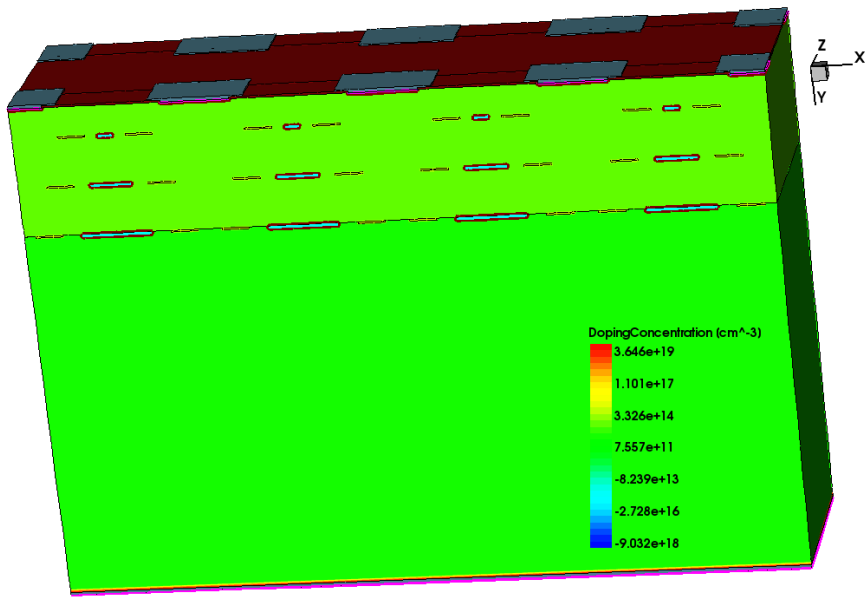


Figure 12: 3D structure of 5x2 n-ELAD sensor

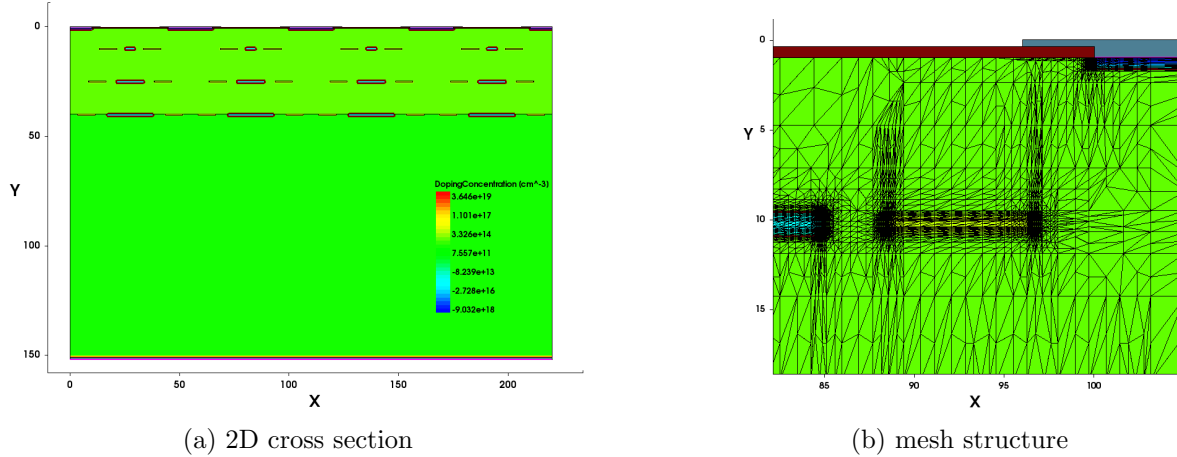


Figure 13: 2D cross section and mesh of 5×2 n-ELAD sensor

3.2 Simulations

After finishing building the 3D structure, electric field simulations and drift simulations are performed on the n-ELAD sensor. The major problem appeared during the simulation process is that fine meshing requires too much memory from SDEVICE. However, when the meshing parameters are large, electric field simulation can't reach depletion voltage. Figure 14 and 15 show the results of the electric field simulation of a half-depleted (150 V) n-ELAD sensor. Although depletion voltage is not reached, the structure of non-homogeneous lateral electric field is already visible for the first two implant layers. The mesh parameters in this case have a minimum of $0.1 \mu\text{m}$ and a maximum of $15 \mu\text{m}$ in x, y, and z direction.

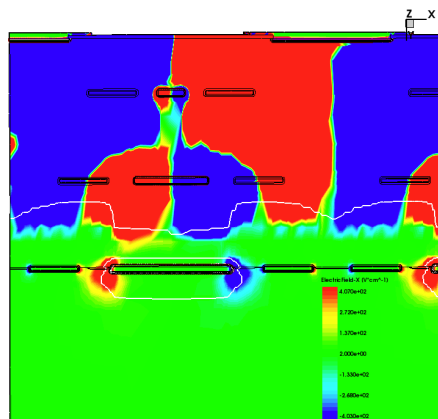


Figure 14: 2D cross section of electric field of half depleted 5×2 n-ELAD sensor

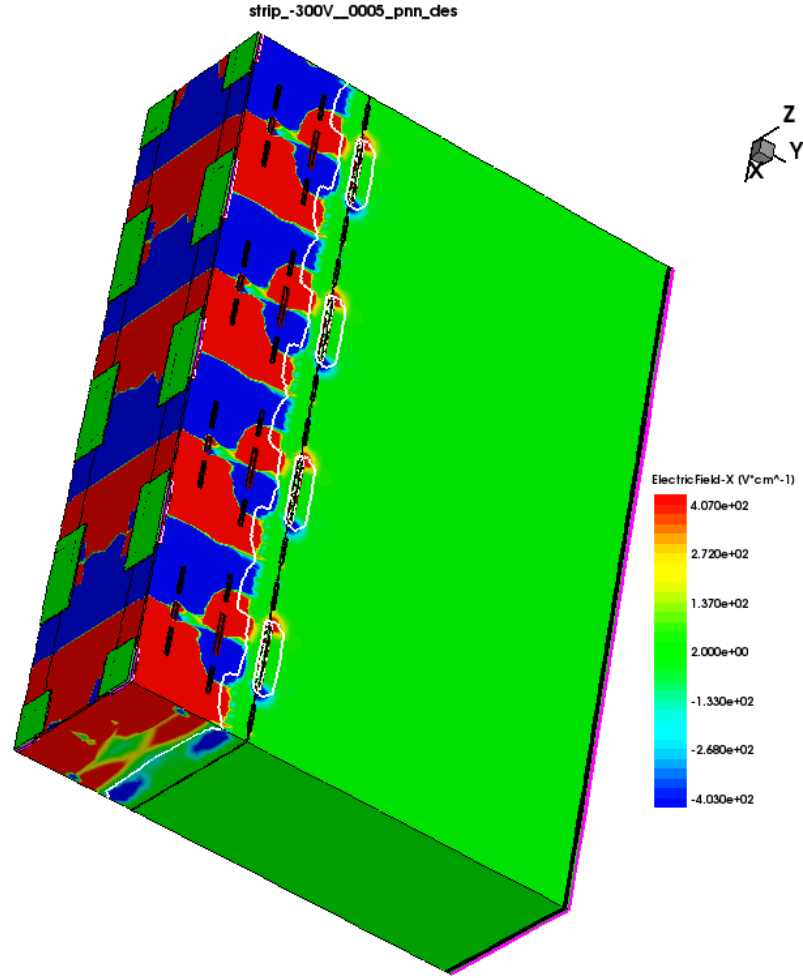


Figure 15: electric field of half depleted 5×2 n-ELAD sensor

The current attempts to try to solve this dilemma are building smaller model and applying different mesh implementation (Figure 16(a) and Figure 17). A small model of $2 \times \frac{1}{2}$ n-ELAD structure is built for trying to get a fully depleted electric field profile. The implants (both readout and deep implants) are surrounded by fine-mesh refinement windows slightly bigger than the implants themselves, while the rest of the sensor has larger mesh parameters, so that the effects of the implants can be simulated without creating too many vertices inside the whole structure. The first attempts with such measures have shown some improvement, the electric field simulation now able to reach 180 V instead of 170 V (Figure 16(b)). The fine mesh parameters for implants in this case have a minimum of 0.1 μm and a maximum of 10 μm , and the broader mesh parameters for other areas have a minimum of 0.054 μm and a maximum of 2 μm .

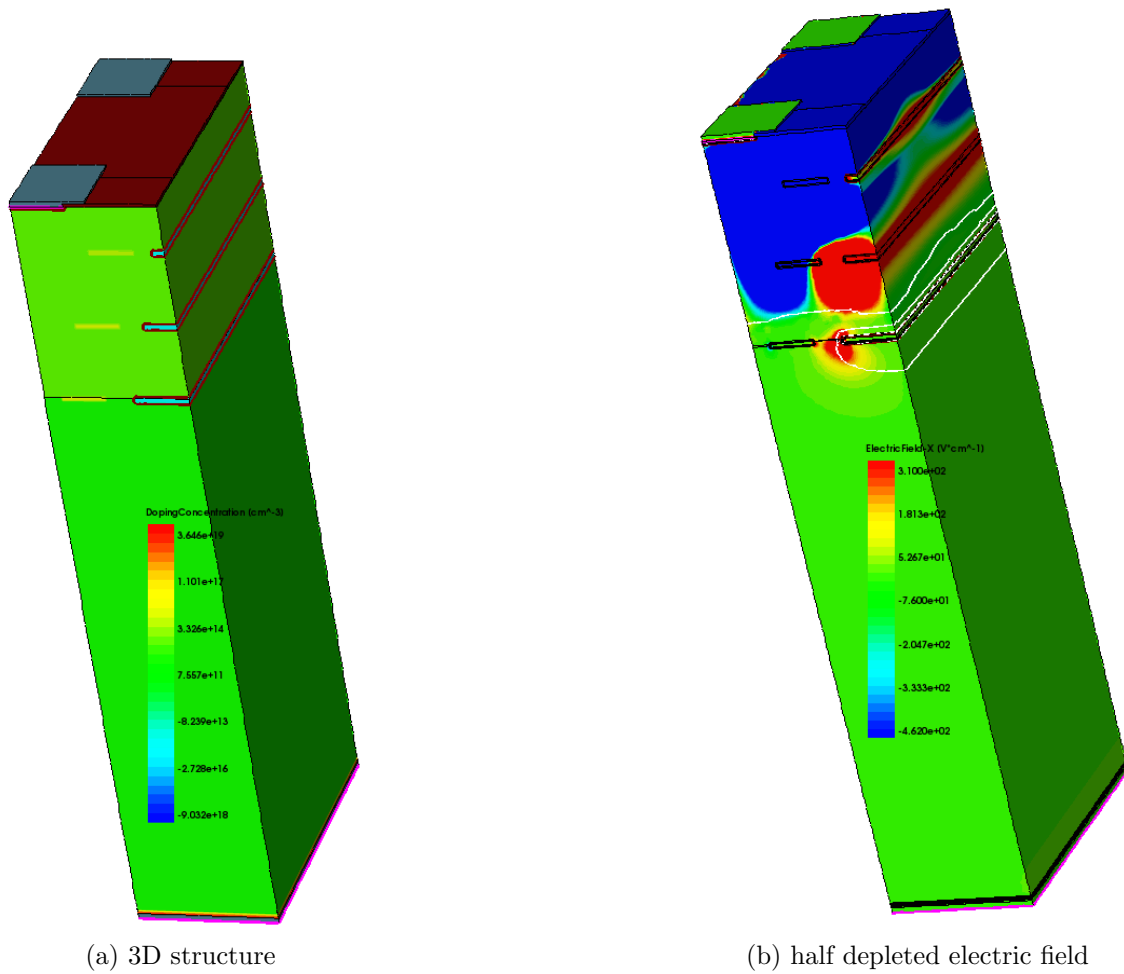


Figure 16: 3D structure and electric field of $2 \times \frac{1}{2}$ n-ELAD sensor

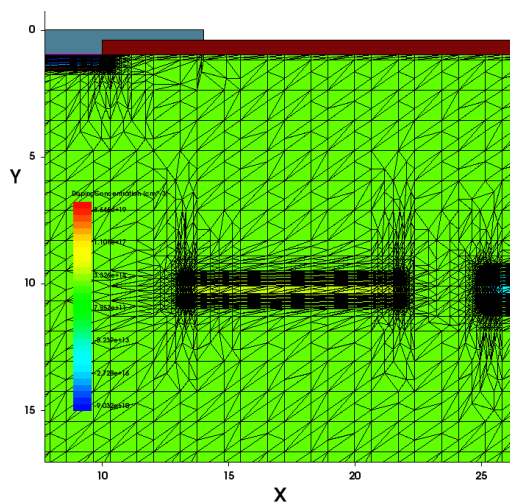


Figure 17: mesh structure of $2 \times \frac{1}{2}$ n-ELAD sensor

4 Summary and Future steps

Building 3D geometric structures of enhanced lateral drift (ELAD) sensors with TCAD SYNOPSIS has been successful for both p-ELAD and n-ELAD sensors. The device simulations, on the other hand, had more difficulties achieving satisfactory results mainly due to the significantly bigger volumes of 3D models comparing to 2D models. But the successfully generated half-depleted electric field simulation does consolidate the fact that deep implants create non-homogeneous electric fields inside ELAD sensor. For future simulations, a better balance between the volume of the whole structure and the mesh parameters needs to be found in order to accommodate the computing capability of TCAD SYNOPSIS. The bigger models also have a problem of exceeding the maximum number of vertices (200,000 vertices) of the TCAD SDE tool. A mesh can still be created by TCAD but the final mesh might not be Delaunay. The effect of this compromise is still not clear and whether it contributes to the difficulties of following device simulations needs further simulation studies.

5 Acknowledgement

First of all, I would like to thank all the organization staff at DESY for granting me this fantastic opportunity to participate in this summer program. I am also thankful for everyone in the DESY CMS group for being welcoming and friendly. A special thank you goes to my supervisor Anastasiia Velyka, who is very nice and patient and is always there to help me with any question. And last but not least, I want to thank all the summer students for making this experience less stressful and so much fun.

References

- [1] Velyka, A., Jansen, H. (2017). *Enhanced lateral drift sensors: concept and development*. Deutsches Elektronen-Synchrotron DESY, Hamburg, Germany.
- [2] Lutz, G. (2007). *Semiconductor radiation detectors: Device physics: with 11 tables*. Berlin: Springer. ISBN: 978-3-540-71678-5.
- [3] Kolbinger, B. (2012). *Simulation of a Silicon-Strip Detector*. HERPHY, Institute of High Energy Physics.
- [4] Jansen, H. (2016). “A pascalian lateral drift sensor”, *Nuclear Instruments and Methods in Physics Research Section A: Accelerators, Spectrometers, Detectors and Associated Equipment*, vol.831, no.1, pp.242-245, proceedings of the 10th International Hiroshima Symposium on the Development and Application of Semiconductor Tracking Detectors.